TED Plaza

Exploring Microstructure Dependencies in Solid Oxide Cells: Leveraging Machine Learning for Enhanced Understanding

Anna Sciazko

The University of Tokyo, Project Research Associate
Institute of Industrial Science
sciazko@iis.u-tokyo.ac.jp

1. Solid Oxide Cells

Demand for clean, sustainable and efficient energy sources has become increasingly urgent due to climate change concerns and the need for energy security and independence. Solid oxide cells (SOCs) are electrochemical energy conversion devices which can operate in two different operating modes; solid oxide fuel cells (SOFCs) and solid oxide electrolysis cells (SOECs). They are very promising technologies for future energy market thanks to the high energy conversion efficiency, low emissions, and fuel flexibility. In particular, high operating temperature of SOCs of 600 – 1000 ºC gives an opportunity for direct feeding of carbon containing fuels such as natural gas and biogas etc. (Minh, 2004; Sharma et al., 2016). SOCs have a great potential for wide range of applications due to their scalability. During SOFC operation, supplied fuel is converted into electricity. On the other hand, H_2 and CO can be produced from H_2O and CO_2 when SOC is operated in the electrolysis mode. SOECs can be a great supplement for fluctuating renewable sources, where the surplus electricity is used for electrolysis operation (Fig. 1). Therefore, when SOCs are operated in the reversible mode they can help in balancing between power supply and demand.

SOC consists of three primary components, i.e. fuel and air electrodes and an electrolyte. The basic principle of electrochemical processes in SOCs are as follows:

SOFC operation:

Fuel electrode reaction: $H_2 + O^{2-} \rightarrow H_2O + 2e^-$ (1)

Oxygen electrode reaction: $0.5O_2 + 2e^- \rightarrow O^{2-}$ (2)

SOEC operation:

Fuel electrode reaction: $H_2O + 2e^- \rightarrow H_2 + O^{2-}$ (3)

Oxygen electrode reaction: $O^{2-} \rightarrow 0.5O_2 + 2e^-$ (4)

Microstructure of the porous electrodes contributes to both initial performance and long-time stability of SOCs. For example, the structure of fuel electrode has to accommodate transports of oxygen ions, electrons, fuel and steam gas species. Conventionally, nickel (Ni)-based composites, such as Ni-yttria stabilized zirconia (Ni-YSZ) and Ni-gadolinium doped ceria (Ni-GDC) are used as fuel electrodes. Typical particle size in the SOFC electrode is in the micrometer and

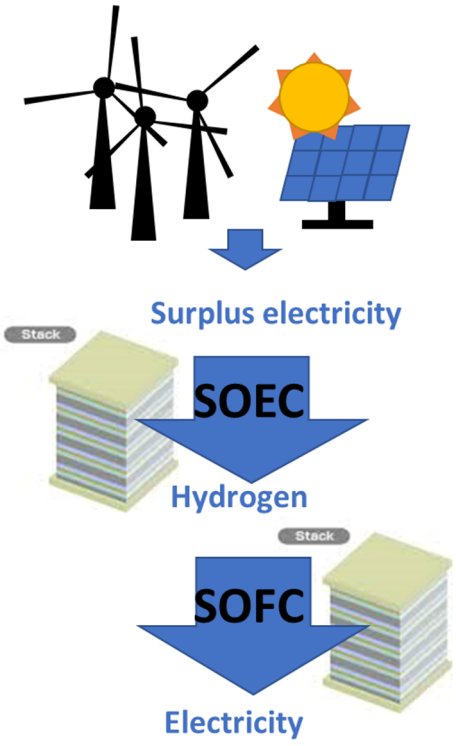

Fig. 1 Operation schema of SOFC and SOEC.

sub-micrometer range. The electrochemical reaction occurs at the boundaries between pore, ion and electron conducting materials, which is called triple phase boundaries (TPBs). For mixed ionic-electronic materials (MIECs), electrochemical reactions can additionally take place on the double phase boundaries (open surface of MIEC particles). Electrochemical reaction sites are schematically shown in Fig. 2 together with an example of typical SOC fuel electrode microstructure.

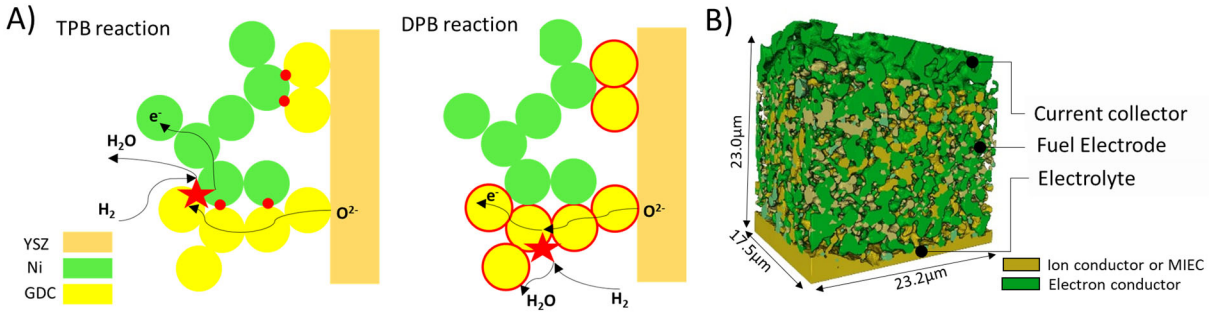

Fig. 2 A) Triple phase boundary (TPB) and double phase boundary (DPB) electrochemical reactions in the fuel electrode and B) typical microstructure of fuel electrode.

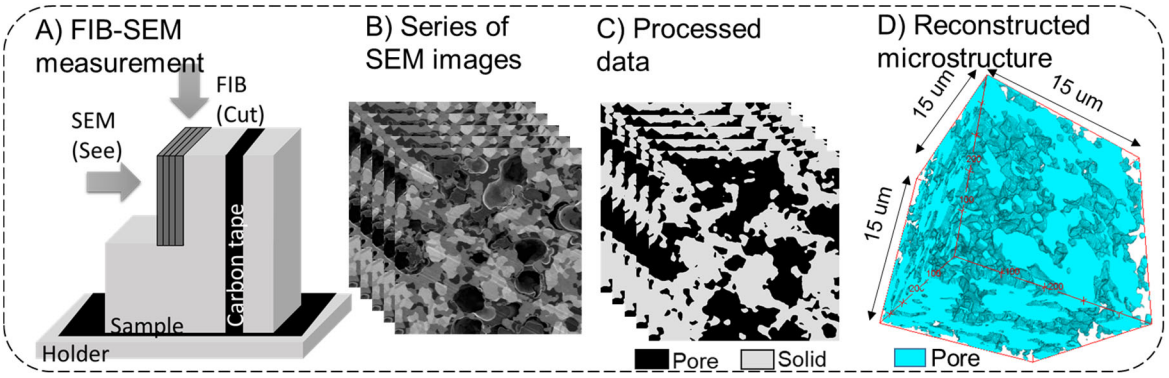

Fig. 3. Microstructure reconstruction by FIB-SEM: A) orthogonal FIB-SEM, B) dataset of SEM images, C) segmented images and D) reconstructed microstructure.

2. FIB-SEM measurements

Three-dimensional (3-D) reconstruction of the microstructure is an important task in the field of material engineering. By obtaining 3-D information, not only the microstructure parameters are calculated, but also the 3-D numerical simulations for transport phenomena can be conducted. The microstructural analyses by focused ion beam-scanning electron microscope (FIB-SEM) can provide detailed and reliable structural information for samples with feature size of 0.01 - 30 μm (Fig. 3). During FIB-SEM measurement, 500 to 1000 sequentual SEM images are taken, processed and assembled into a 3-D model. FIB-SEM has been successfully applied in the field of SOC for evaluating relationships between the microstructure, electrochemical performance and microstructural degradation, e.g. initial structure influence (Kishimoto et al., 2011; Sciazko et al., 2022) Ni reduction (de Angelis et al., 2020), redox stability (Pecho et al., 2015), coarsening (Chen-Wiegart et al., 2016), migration (Nakajo et al., 2020; Ouyang et al., 2022), ceramic support deformation (Komatsu et al., 2021; Zekri et al., 2017), sulfur poisoning (Harris et al., 2014), and carbon deposition (Sciazko et al., 2023), etc.

However, quantitative evaluations of microstructures are still very challenging, as it requires reliable data segmentation algorithms as well as large reconstruction volume and high resolution of imagining. There is a trade-off between reconstruction volume and resolution as shown in Fig. 4 (Xu et al., 2017), where the typical scale of relevant SOC microstructure features covers several orders of magnitude (Wankmüller et al., 2020). In addition, FIB-SEM measurement requires collecting a large number of consecutive SEM images. Therefore, FIB-SEM is not feasible for fast screening due to the measurement complexity.

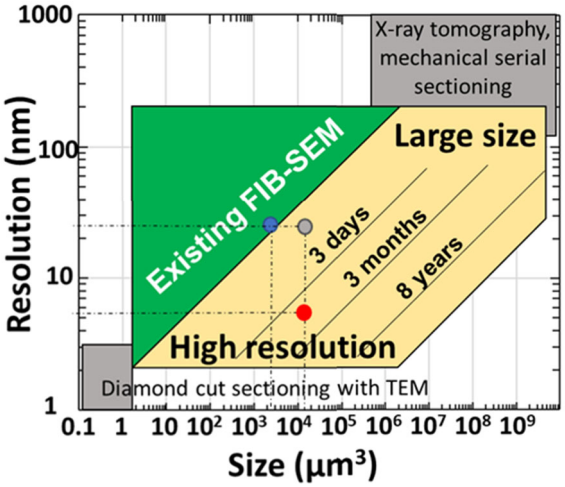

Fig. 4 Limitations of FIB-SEM measurement. The lines indicate theoretical time dependence between resolution and reconstruction size (Xu et al., 2017).

Machine learning has emerged as a powerful tool for understanding and analyzing complex data for materials engineering (Schmidt et al., 2019; Wei et al., 2019). Machine learning techniques is expected in the characterization of SOC microstructures, which may finally help in developing improved electrodes. The approach by deep neural network can potentially overcome FIB-SEM limitations and provide high resolution-large volume 3-D reconstruction. The previous works concentrated on relatively simple artificial neural networks (ANN), but convolutional neural networks (CNN) can effectively analyze the visual imagery. Recently, Hwang et al. demonstrated a segmentation of fuel cell microstructure by deep learning based on DeebLabV3+ algorithm (Hwang et al., 2020). However, the achieved pixel-based accuracy was only 78%. Wu et al. (2019) demonstrated that the diffusivity of porous structure can be predicted from a 2-D image by CNN, but they did not provide the method to fabricate a 3-D model. Gayon-Lombardo et al. (2020) demonstrated the successful application of generative adversarial networks (GAN) to fabricate synthetic SOFC microstructures. Their result proved that GAN-based approach can be very effective, but the algorithm required the 3-D teaching data and could not fabricate microstructures with pre-defined properties.

3. Application of machine learning methods for SOC microstructures

Here, the strategy for improving the FIB-SEM measurements with machine learning methods is presented. All experimental microstructural samples are from the previously measured SOFC and SOEC cells. The proposed methods focus on three major points: (I) automated segmentation of multi-phase porous microstructures (II) improving resolution of microscopic images and (III) generating artificial 2-D and 3-D microstructures.

3.1. Semantic segmentation

A machine learning assisted image processing framework for the automatic segmentation of large datasets of raw FIB-SEM images was developed (Sciazko et al., 2021). The algorithm adopted a patch-based convolutional neural network (patch-CNN) in the encoder-decoder configuration as shown in Fig. 5. The proposed network was utilized for the segmentation of resin infiltrated cross-sectional images, which enabled reduction in processing time from days to hours with accuracy over 98%. The overall pixel accuracy, the numbers of training and total SEM images of various samples are shown in Table 1.

The patch-CNN was extended for double-step U-net network for processing SEM data without resin infiltration (Sciazko et al., 2023). This algorithm was applied to investigate the 3D structures of the deposited carbon in the fuel electrode. Carbon deposition is considered to be one of important degradation mechanisms in SOFC system operated with hydrocarbon fuels. This first-of-its-kind work enabled to quantitatively evaluate the carbon deposition and its influence on degradation. An example of carbon deposition in Ni-GDC sample is shown in Fig. 6.

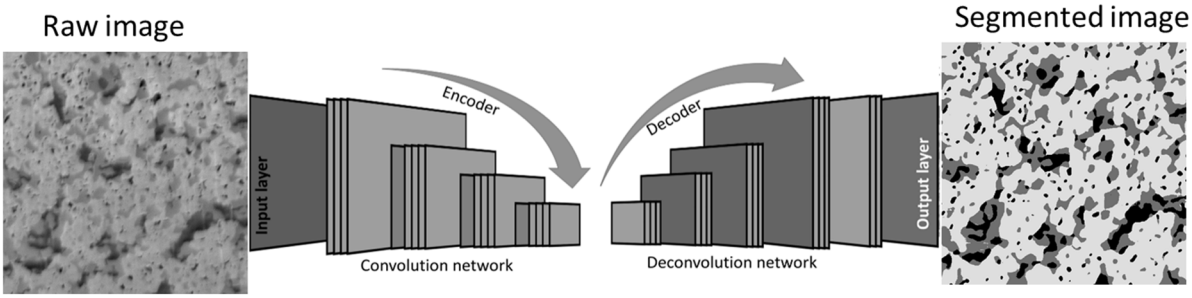

Fig. 5 Schematic of patch-based semantic segmentation network in encoder-decoder configuration.

Table 1 Accuracies and number of images of semantic segmentation networks trained for various microstructures (Sciazko et al., 2021).

Sample		Overall pixel accuracy, OP -	SEM images	Training images	Number of training image / Total slices
LSCM-GDC 5050 (1200°C)		0.971	601	9	0.015
LSCM-GDC 50:50 (1100°C)		0.975	779	9	0.011
Ni-GDC		0.982	980	97	0.099
Ni-YSZ-AS	Pore filling	0.969	934	3	0.003
	Ternarization	0.969	934	17	0.018

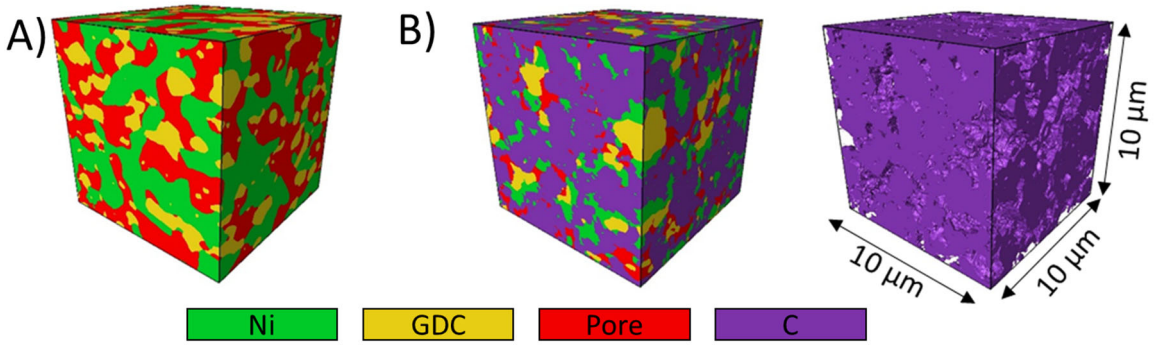

Fig. 6 3D reconstruction of Ni-GDC microstructure; A) initial and B) after carbon deposition experiment.

3.2. Super-resolution

The voxel size in FIB-SEM reconstruction is determined by the SEM image resolution and FIB slicing pitch. To achieve high quality 3D reconstruction, it is necessary to set narrow FIB slicing pitch, which results in large number of captured SEM images and long measurement time. Here, a new method for artificially increasing the number of slices in FIB-SEM image stack is proposed by implementing asymmetric-resolution algorithm (Sciazko, Komatsu, Shimura, et al., 2021a). The residual deep neural network based on a modified VDSR architecture (Kim et al., 2016) is used to increase the resolution in the FIB slicing direction. The schematic illustration of VDSR network is shown in Fig. 7.

An example of applying VDSR network in FIB-SEM data is shown in Fig. 8. The FIB slicing pitch of 200 nm is 8 times larger than the SEM resolution of 25 nm. The VDSR network firstly learns the mapping between low- and high-resolution data based on the SEM images. Trained network is later applied to generate sub-images in the stacking direction. This mapping is possible because low- and high-resolution images have similar features, and the VDSR has to reproduce only the high-frequency details in a single direction. The proposed algorithm can significantly shorten the FIB-SEM measurement time or increase the measurement volume maintaining high resolution.

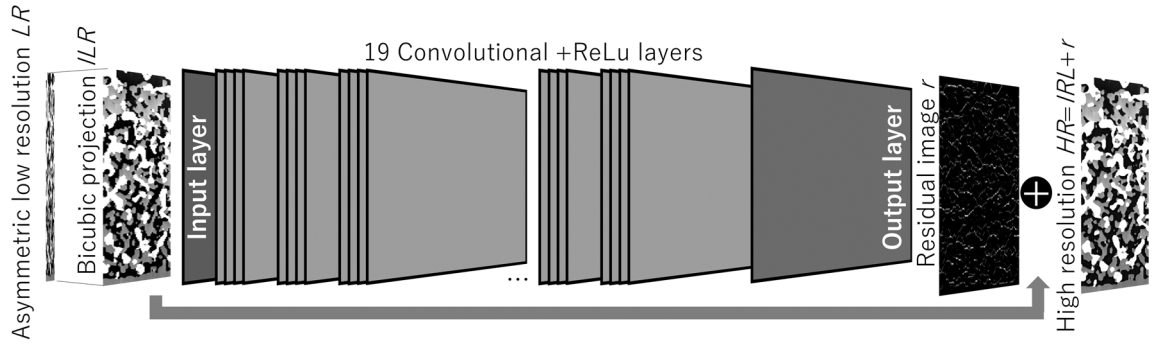

Fig. 7 Schematic of patch-based residual VDSR network (Sciazko, Komatsu, Shimura, et al., 2021a).

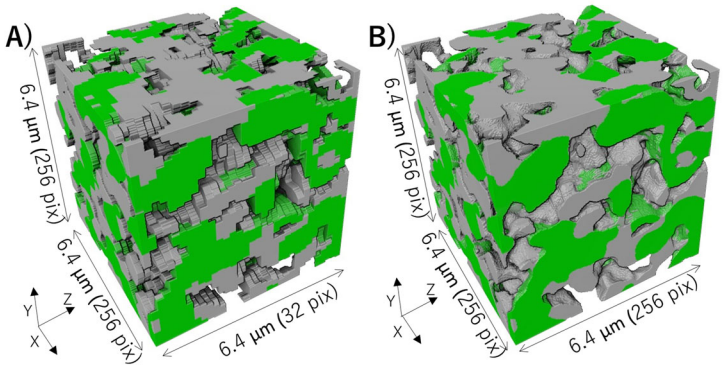

Fig. 8 Comparison of microstructures between A) original anisotropic FIB-SEM with 25 × 25 × 200 nm resolution and B) VDSR microstructure with 25 × 25 × 25 nm resolution (Sciazko, Komatsu, Shimura, et al., 2021a).

3.3 Artificial microstructures

The generative machine learning can produce artificial structures with predefined statistical properties. Conventionally, generated structures belonged to the same class as the training data. For example, if 2-D images are used for training, the GAN network generates 2-D structures (GAN^{2D-2D}) as shown in Fig. 9, and the network trained by 3-D data will provide 3-D structure (GAN^{3D-3D}).

Here, an new algorithm for generating 3-D structures from 2-D cross sectional SEM image as a training data (GAN^{2D-3D}) is proposed as shown in Fig. 10 (Sciazko, Komatsu & Shikazono, 2021). The proposed GAN network is composed of a 3-D generator and a 2-D discriminator. Primarily, the model is designed for the isotropic structures as shown in Fig. 11A. Then, weak GAN^{2D-3D} network was further developed for anisotropic materials enabling reconstructing electrode microstructures with electrolytes as shown in Fig. 11B. Both visual quality and statistical characteristics of the artificial models are in very good agreement with the real data.

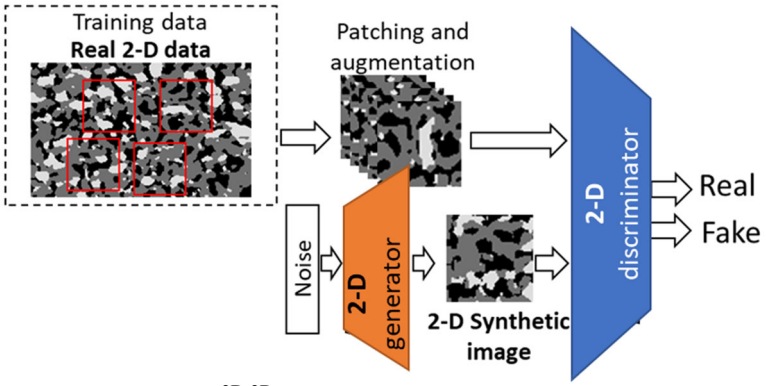

Fig. 9 Structure of GAN^{2D-2D} network (Sciazko, Komatsu & Shikazono, 2021).

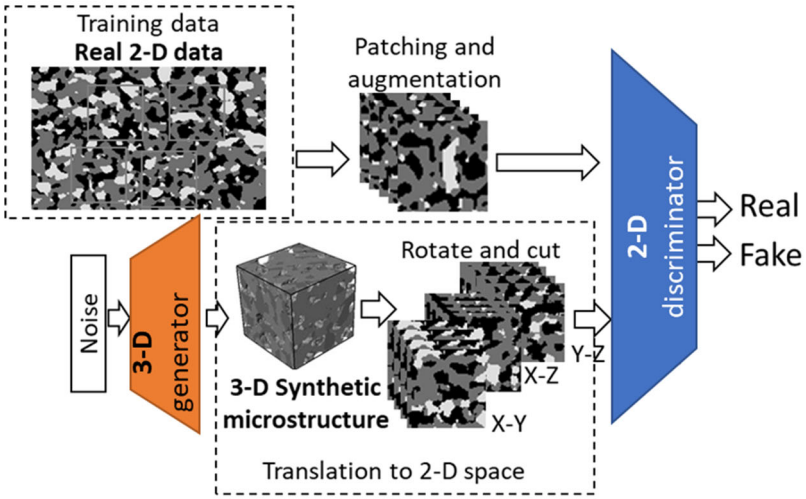

Fig. 10 Structure of GAN$^{2D\text{-}3D}$ network (Sciazko, Komatsu, & Shikazono, 2021).

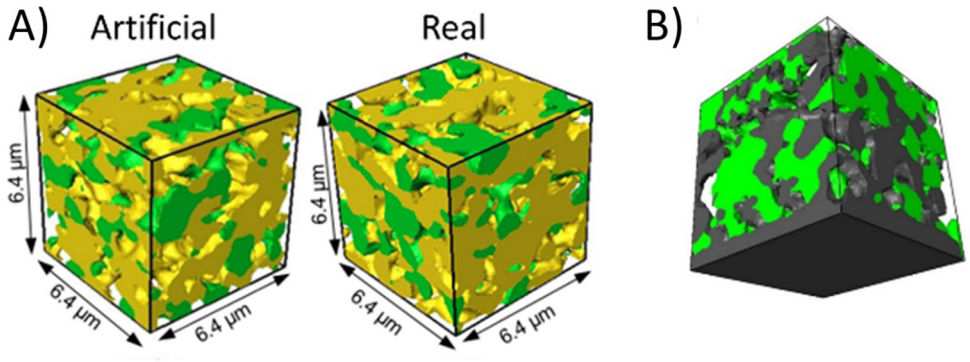

Fig. 11 Reconstructed 3-D microstructures from 2-D cross sectional images by GAN$^{2D\text{-}3D}$ network: A) isotropic microstructure and B) microstructure with electrolyte (Sciazko, Komatsu & Shikazono, 2021).

4. Summary and conclusion

Coupling machine learning and FIB-SEM measurements makes it possible to reveal new properties of SOCs microstructures. In the present study, three types of algorithms are proposed, i.e. semantic segmentation of raw SEM data, super-resolution for improving resolution of FIB-SEM measurements and fabrication of artificial microstructures. These methods enable reduction in FIB-SEM measurement time by 8 times and data post-processing time is reduced by a factor of hundred. In addition, it become possible to synthesize 3D microstructure directly from 2D cross sectional data. Here, applications of machine learning to FIB-SEM images are introduced. It is expected that machine learning will have more future applications such as degradation prediction.

Acknowledgements

This work was partly supported by the New Energy and Industrial Technology Development Organization (NEDO), by Japan Society for the Promotion of Science KAKENHI [grant number 23K13261] and by Advanced Research Infrastructure for Materials and Nanotechnology in Japan (ARIM Japan).

References

Chen-Wiegart, Y. K., Kennouche, D., Scott Cronin, J., Barnett, S. A., & Wang, J. (2016). Effect of Ni content on the morphological evolution of Ni-YSZ solid oxide fuel cell electrodes. Applied Physics Letters, 108(8), 083903.

de Angelis, S., Jørgensen, P. S., Tsai, E. H. R., Holler, M., Fevola, G., & Bowen, J. R. (2020). Tracking nickel oxide reduction in solid oxide cells via ex-situ ptychographic nano-tomography. Materials Characterization, 162, 110183.

Gayon-Lombardo, A., Mosser, L., Brandon, N. P., & Cooper, S. J. (2020). Pores for thought: generative adversarial networks for stochastic reconstruction of 3D multi-phase electrode microstructures with periodic boundaries. Npj Computational Materials, 6(1), 1–11.

Harris, W. M., Lombardo, J. J., Nelson, G. J., Lai, B., Wang, S., Vila-Comamala, J., Liu, M., Liu, M., & Chiu, W. K. S. (2014). Three-dimensional microstructural imaging of sulfur poisoning-induced degradation in a Ni-YSZ anode of solid oxide fuel cells. Scientific Reports, 4, 1–7.

Hwang, H., Choi, S. M., Oh, J., Bae, S. M., Lee, J. H., Ahn, J. P., Lee, J. O., An, K. S., Yoon, Y., & Hwang, J. H. (2020). Integrated application of semantic segmentation-assisted deep learning to quantitative multi-phased microstructural analysis in composite materials: Case study of cathode composite materials of solid oxide fuel cells. Journal of Power Sources, 471(May), 228458.

Kim, J., Lee, J. K., & Lee, K. M. (2016). Accurate image super-resolution using very deep convolutional networks. Proceedings of the IEEE Computer Society Conference on Computer Vision and Pattern Recognition, 2016-Decem, 1646–1654.

Kishimoto, M., Iwai, H., Saito, M., & Yoshida, H. (2011). Quantitative evaluation of solid oxide fuel cell porous anode microstructure based on focused ion beam and scanning electron microscope technique and prediction of anode overpotentials. Journal of Power Sources, 196(10), 4555–4563.

Komatsu, Y., Sciazko, A., Suzuki, Y., Ouyang, Z., Jiao, Z., & Shikazono, N. (2021). Operando observation of patterned nickel - gadolinium doped ceria solid oxide fuel cell anode. Journal of Power Sources, 516, 230670.

Minh, N. Q. (2004). Solid oxide fuel cell technology - Features and applications. Solid State Ionics, 174(1–4), 271–277.

Nakajo, A., Rinaldi, G., Caliandro, P., Jeanmonod, G., Navratilova, L., Cantoni, M., & van herle, J. (2020). Evolution of the Morphology Near Triple-Phase Boundaries in Ni–Yttria Stabilized Zirconia Electrodes Upon Cathodic Polarization. Journal of Electrochemical Energy Conversion and Storage, 17(4), 1–13.

Ouyang, Z., Komatsu, Y., Sciazko, A., Onishi, J., Nishimura, K., & Shikazono, N. (2022). Operando observations of active three phase boundary of patterned nickel - Yttria stabilized zirconia electrode in solid oxide cell. Journal of Power Sources, 231228.

Pecho, O., Stenzel, O., Iwanschitz, B., Gasser, P., Neumann, M., Schmidt, V., Prestat, M., Hocker, T., Flatt, R., & Holzer, L. (2015). 3D Microstructure Effects in Ni-YSZ Anodes: Prediction of Effective Transport Properties and Optimization of Redox Stability. Materials, 8(9), 5554–5585.

Schmidt, J., Marques, M. R. G., Botti, S., & Marques, M. A. L. (2019). Recent advances and applications of machine learning in solid-state materials science. Npj Computational Materials, 5(1).

Sciazko, A., Komatsu, Y., Nakamura, A., Ouyang, Z., Hara, T., & Shikazono, N. (2023). 3D microstructures of solid oxide fuel cell Ni-YSZ anodes with carbon deposition. Chemical Engineering Journal, 460.

Sciazko, A., Komatsu, Y., & Shikazono, N. (2021). Unsupervised Generative Adversarial Network for 3-D Microstructure Synthesis from 2-D Image. ECS Transactions, 103(1), 1363–1373.

Sciazko, A., Komatsu, Y., Shimura, T., & Shikazono, N. (2021a). Electrode Microstructure Reconstruction from FIB-SEM Datasets with Anisotropic Resolutions. The Proceedings of the National Symposium on Power and Energy Systems 2021.25, C212.

Sciazko, A., Komatsu, Y., Shimura, T., & Shikazono, N. (2021b). Segmentation of Solid Oxide Cell Electrodes by Patch Convolutional Neural Network. Journal of The Electrochemical Society, 168(4), 044504.

Sciazko, A., Komatsu, Y., Yokoi, R., Shimura, T., & Shikazono, N. (2022). Effects of mass fraction of La0.9Sr0.1Cr0.5Mn0.5O3-δ and Gd0.1Ce0.9O2-δ composite anodes for nickel free solid oxide fuel cells. Journal of the European Ceramic Society, 42(4), 1556–1567.

Sharma, M., Rakesh, N., & Dasappa, S. (2016). Solid oxide fuel cell operating with biomass derived producer gas: Status and challenges. Renewable and Sustainable Energy Reviews, 60, 450–463.

Wankmüller, F., Meffert, M., Russner, N., Weber, A., Schmieg, J., Störmer, H., Dickel, T., Lupetin, P., Maier, N., Gerthsen, D., & Ivers-Tiffée, E. (2020). Multi-scale characterization of ceramic inert-substrate-supported and co-sintered solid oxide fuel cells. Journal of Materials Science, 55(25), 11120–11136.

Wei, J., Chu, X., Sun, X., Xu, K., Deng, H., Chen, J., Wei, Z., & Lei, M. (2019). Machine learning in materials science. InfoMat, 1(3), 338–358.

Wu, H., Fang, W. Z., Kang, Q., Tao, W. Q., & Qiao, R. (2019). Predicting Effective Diffusivity of Porous Media from Images by Deep Learning. Scientific Reports, 9(1), 1–12. https://doi.org/10.1038/s41598-019-56309-x

Xu, C. S., Hayworth, K. J., Lu, Z., Grob, P., Hassan, A. M., García-Cerdán, J. G., Niyogi, K. K., Nogales, E., Weinberg, R. J., & Hess, H. F. (2017). Enhanced FIB-SEM systems for large-volume 3D imaging. ELife, 6, 1–36.

Zekri, A., Knipper, M., Parisi, J., Plaggenborg, T., Jurgen, P., & Plaggenborg, T. (2017). Microstructure degradation of Ni/CGO anodes for solid oxide fuel cells after long operation time using 3D reconstructions by FIB tomography. Phys. Chem. Chem. Phys., 19(21), 13767–13777.